Design of a Fault-Tolerant 6-phase Switched Reluctance Motor for Electric Power-Assisted Steering Systems

C. Martis*, C. Oprea*, I.A. Viorel* and J. Gyselinck**
*Technical University of Cluj Napoca
15, Daicoviciu, Cluj-Napoca, RO-400020, Romania
**Université Libre de Bruxelles
50, Avenue Franklin Roosevelt, Brussels, B-1050, Belgium

Abstract – **In this paper a six-phase switched reluctance motor for electric power-assisted steering systems is proposed. Based on the specification data the main motor dimensions are obtained via a dedicated sizing-design procedure. The motor parameters and characteristics are computed by using three methods, namely using a finite element model, a magnetic equivalent circuit model and using analytical formulas. The flux linkage and electromagnetic torque as a function of rotor position and phase current are calculated, showing that the steady state motor characteristics are adequate for the purposed drive.**

I. INTRODUCTION

Electric actuation is one of the actual trends in the automotive industry, due to its high reliability, energy efficiency and controllability [1]. The use of electrical and electronic systems, such as electronic automatic climate control, entertainment systems, antilock brakes (ABS), traction control systems, enhances customer comfort, convenience and safety. New electric systems eliminate the traditional pumps, hoses, hydraulic fluid, drive belt and pulley on the engine, significantly increasing fuel economy.

Electric power-assisted steering (EPAS) systems have already begun replacing the hydraulic power steering ones, simplifying vehicle assembly and offering more room in the engine compartment. An EPAS system incorporates a steering gear, assist mechanism, an electric motor and its electronic controller to provide responsive steering assist. Normally, sensors measure two primary inputs: applied torque on the steering wheel and the position of the latter. EPAS solutions can be separated into categories according to the location of the electric motor that provides steering assistance, as: column-type, pinion-type, rack-type, and double pinion-type [1, 2].

Some aspects have to be considered during the design of the EPAS drive systems: reliability, performance, thermal and acoustic behavior, energy efficiency and cost. These applications require high performance motors with high torque/volume ratio, low inertia, high dynamics, low torque pulsations and low radial forces. Different types of electrical motors have been proposed and used for EPAS applications so far. The first "all electric" power-steering system used a brush DC motor placed concentrically around the rack [1]. But the DC motor has some unattractive attributes, such as brush arcing and commutator/brush friction, resulting in wear, lower overall power density and EMI problems.

As a result, the robust induction motor was chosen to replace brush DC motor in EPAS applications. The difficulties associated with extracting heat from the rotor, efficiency problems over a wide speed range if high slip is required, long end-turns, and a more expensive manufacturing process due to the distribution of windings are some of the unattractive features of the induction machine that made researchers look for other solutions. The permanent magnet synchronous machine (PMSM) represents a competitive solution for the considered application. High torque density, low cogging torque, small torque ripple and high energy efficiency are the key assets of PMSMs for this kind of application [2].

However, high power density permanent magnets are extremely sensitive to the temperature increase, the stability temperature limit being well below 120°C. This is to be taken into consideration since in automotive applications the ambient temperature limits are from -40°C up to 125°C and more. The PMSMs also raise concerns about failure modes and, without an adequate design and control, can produce quite important cogging torques.

Switched reluctance machines (SRMs) are easy to construct and contain no permanent magnets, resulting in excellent high-temperature performance and high reliability. Due to the phase independence, SRMs are able to operate under partial phase failure conditions and therefore are a competitive candidate for fault tolerant EPAS applications, where safety is the most important consideration.

The analysis of the specifications for automotive EPAS reveals also some other interesting motor challenges: given overall dimension, low supply voltage, wide range of ambient temperature, and low motor torque ripple.

The fault tolerance of an EPAS system can be focused either on the power electronic converter, or on the electrical machine. Concerning the latter, the effort can be oriented towards the windings and the number of phases, without increasing the complexity of the drive. The minimization of the torque ripple

978-1-4244-4252-2/09/$25.00 ©2009 IEEE

can also be tackled in two ways, i.e. by optimizing the motor design and/or by improving the control strategy.

While low cost, robust structure, low inertia, high reliability and controllability are some of the SRM characteristics that make it suitable for EPAS applications, the high ripple content of the developed electromagnetic torque is an important drawback. Designing a SRM drive for EPAS systems should then envisage some constraints, mainly focused on the minimization of the torque ripple.

Following the specific EPAS requirements, the present paper approaches the design and analysis of a 12/10 6-phase SRM for a fault tolerant EPAS application, using the finite element method (FEM) [9], a magnetic equivalent circuit model and analytical formulas.

The main dimensions of the machine are calculated by using a preliminary sizing procedure based on the output power equation [3, 4]. The machine parameters will be calculated using three approaches, using a finite element model, a magnetic circuit model and analytical formulas, respectively, and the results will be compared.

II. Design of The Switched Reluctance Machine

The specification data and the demanded torque-speed curve for the electric motor of a column-type EPAS system as described in literature [2] are presented in Table I and Figure 1.

TABLE I

Specification data for the electric motor of an EPAS System

Peak stall torque (T)	7Nm
Base speed (n_N)	500rpm
Maximal speed (n_{max})	3000rpm
DC-bus voltage (U)	12V
Duty cycle	S3-5%
Ambient temperature	-40...125°

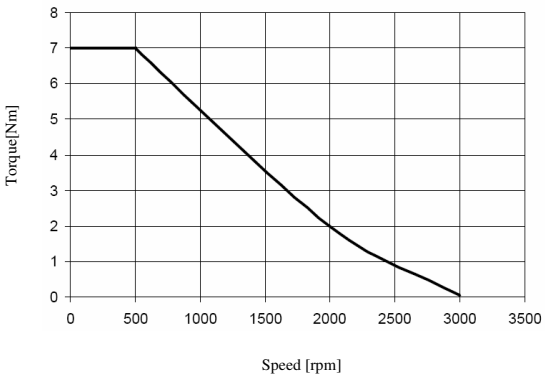

Figure 1. Torque vs speed curve for an EPAS system.

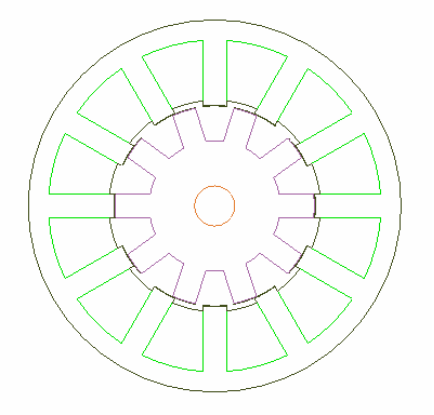

Figure 2. Cross section of the proposed SRM.

For a low ripple content and higher fault-tolerant SRM, two very important aspects must be considered: pole and phase number. The high ripple content of the electromagnetic torque for SRM is due to the doubly salient structure and the non-linear flux linkage vs current characteristic.

Considering the relationship between stator and rotor pole numbers (Q_S, respectively Q_R) for regular SRMs:

$$Q_R = Q_S \pm 2 \tag{1}$$

a 12/10 pole topology was chosen.

Even if three-phase machines are the most common electrical drives, a 6-phase configuration was chosen in order to reduce the torque ripple and to improve the fault tolerance of the system. The cross section of the proposed SRM is presented in figure 2.

The design procedure should start with a preliminary sizing which offers the initial main dimensions of the machine. The main sizing equation is the well-known $D_g^2 l_S$ equation, named the output power equation, relating the machine dimensions to the magnetic and electric loading. Thus, the output power for an electrical machine is proportional to the product of specific electric and magnetic loadings, airgap diameter and effective stack length [5]:

$$P_{out} = \frac{Q_R}{Q_S}\pi^2 \eta K_L K_I A_S n_N B_{g\,max}\left(1 - \frac{1}{K_C}\right) D_g^3 \tag{2}$$

with the required output power of the machine given by:

$$P_{out} = T\frac{\pi n_N}{30} \tag{3}$$

where η is the machine efficiency, A_S the stator electrical loading, B_{gmax} the maximum value of the airgap flux density (1.2 to1.8T, depending on the lamination quality), D_g, the machine airgap diameter, K_I the current waveform factor [4], K_C, Carter's factor (1.4…1.8 for preliminary sizing procedure) and K_L, the aspect ratio coefficient, given by:

$$K_L = \frac{l_S}{D_g} \tag{4}$$

with l_s the effective stack length. Following the overall dimension constraint, the aspect ratio coefficient K_L will be imposed at 1.25. The same constraint will limit the outer stator diameter to 150 mm maximum value.

The stator airgap diameter will be calculated as:

$$D_g = \sqrt[3]{P_{out} \frac{Q_S}{Q_R \pi^2 \eta K_L K_I A_S n_N B_{g\,max} \left(1 - \frac{1}{K_C}\right)}} \tag{5}$$

The pole pitch, pole width and yoke height for both stator and rotor are given by [5]:

$$\begin{aligned} \tau_{pi} &= \pi \frac{D_i}{Q_i} \\ b_{pi} &= (0.8...1)\frac{\tau_{pi}}{2}, i = S, R \\ h_{yi} &= (0.8...1)\frac{b_{pi}}{2} \end{aligned} \tag{6}$$

The stator pole geometry has to allow for the insertion of the prewound coils and to provide enough slot area for the stator winding. The number of turns per phase results from:

$$N_{ph} = round\left(2gK_{sat}\frac{B_{g\,max}}{\mu_0 k_\sigma I}\right) \tag{7}$$

with k_σ the leakage flux factor (between 0.75 and 1), g the airgap length and I the phase current given by:

$$I = \frac{P_{out}}{U \cos\varphi} \tag{8}$$

for one-on-phase supply strategy, where cosφ is the equivalent power factor of the machine (0.7…0.85, without power factor correction circuit). For the preliminary design, the equivalent power factor was considered 0.83.

Considering the slot fill factor, $k_{fill,}$ and the area occupied by the winding, A_{wind}, the slot area will be:

$$A_{slot} = \frac{A_{wind}}{k_{fill}} \tag{9}$$

where k_{fill} = 0.35…0.55, and

$$A_{wind} = \frac{N_{ph} I}{2 * J} \tag{10}$$

J, the current density (5…8 A/mm^2), with the maximum value considered.

The stator pole height, h_{pS}, will then result from:

$$h_{pS}\left[\frac{\pi(D_g + g + 2h_0 + h_{pS})}{Q_S} - b_{pS}\right] = A_{wind} \tag{11}$$

where g is the airgap length (0.2…1 mm, depending on the output power of the machine) and h_0 is the wedge thickness. The rotor pole height results from:

$$h_{pR} = \frac{D_g}{2} - h_{yR} - \frac{D_{shaft}}{2} > 20g \tag{12}$$

with h_{yR} the height of the rotor yoke and D_{shaft} the shaft diameter.

The resulting main dimensions of the machine are presented in Table II.

TABLE II
MAIN DIMENSIONS OF THE MACHINE

Stator outer diameter	148 mm
Stator inner diameter	80 mm
Airgap	0.5 mm
Stack length	100 mm
Stator pole width	9.4 mm
Stator pole height	26 mm
Rotor pole width	9.4 mm
Rotor pole height	17mm

III. MACHINE ANALYSIS AND PARAMETERS COMPUTATION

The key dimensions of the machine being determined, the next step in the design procedure will consider the analysis and computation of machine performances and parameters. The electromagnetic torque, phase flux linkage and phase inductance will be computed using three models (finite element model, magnetic circuit model and analytical model).

A. *FEM analysis*

So, using the design procedure results, a model of the proposed SRM was developed, and analyzed for different phase current values and different rotor positions, using a FE method. The magnetic flux patterns for aligned (θ=0º) and unaligned (θ=18º) positions are presented in Figures 3 and 4.

The phase flux linkage for aligned (θ=0º), unaligned (θ=18º) and midway (θ=9º) rotor positions is presented in Figure 5, as function of stator current.

The one-phase developed electromagnetic torque as function of rotor position and stator current (4A, 12A, 20A, 28A, 36A) is presented in Figure 6.

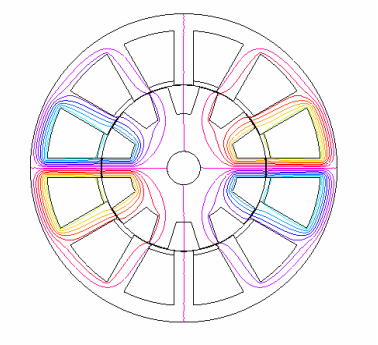

Figure 3. Magnetic flux path for θ=0º (aligned position).

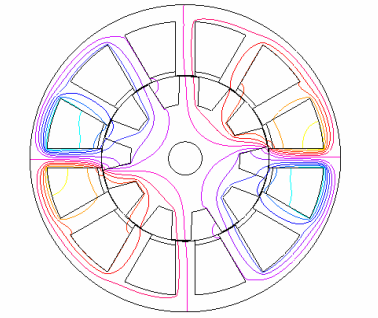

Figure 4. Magnetic flux path for θ=18º (unaligned position).

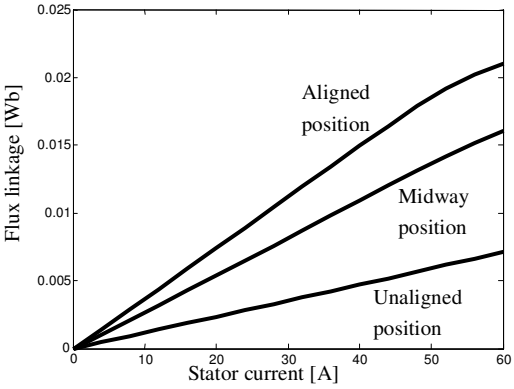

Figure 5. Flux linkage vs stator current.

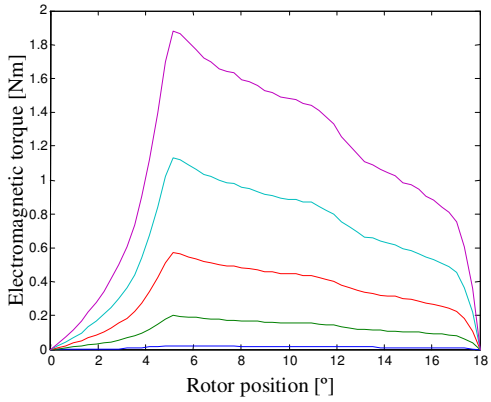

Figure 6. Electromagnetic torque vs rotor position and phase current.

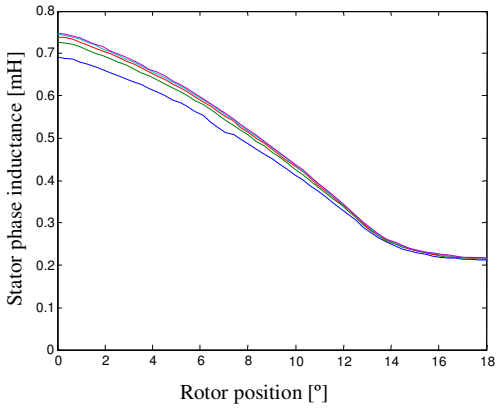

Figure 5. Phase inductance vs rotor position and phase current.

The phase inductance can be derived as:

$$L_{ph}(i,\theta)=\left.\frac{\partial\Phi(i,\theta)}{\partial i}\right|_{\theta=cst} \tag{13}$$

and it is presented in Figure 5 for five different stator current values current (4A, 12A, 20A, 28A, 36A).

B. Magnetic equivalent circuit analysis

The phase inductance can be computed using the magnetic equivalent permeance for one pole, expressed as a function of the rotor displacement θ [5]:

$$P(\theta)=P_0+P_1\cos(Q_R\theta) \tag{14}$$

where the expressions of the coefficients P_0 and P_1 are:

$$P_0=\frac{\mu_0 b_{ps} l_s}{gK_C}$$
$$P_1=P_0\frac{Q_s}{\pi}\lambda_R\left(\frac{1}{Q_R}+\frac{\lambda_S Q_R}{Q_S^2-Q_R^2}\right)\sin\left(\frac{Q_R}{Q_S}\pi\right) \tag{15}$$

with λ_S and λ_R, airgap permeance coefficients [5] and $K_{C(S,R)}$ the computed stator/rotor Carter's factor :

$$\lambda_i=\frac{4}{\pi}\beta_i K_{Ci}\sin\left(\frac{\gamma_i g\pi}{2\beta_i\tau_{pi}}\right),\quad K_{Ci}=\frac{\tau_{pi}}{\tau_{pi}-\gamma g}\text{ , i=S,R} \tag{16}$$

with

$$\gamma_i=\frac{4}{\pi}\left[\frac{b_{pi}}{2g}\arctan\left(\frac{b_{pi}}{2g}\right)-\ln\sqrt{1+\left(\frac{b_{pi}}{2g}\right)^2}\right],\ \text{i=S,R} \tag{17}$$
$$\beta_i=\frac{(1-f_i)^2}{2(1+f_i^2)},\ f_i=\frac{b_{pi}}{2g}+\sqrt{1+\left(\frac{b_{pi}}{2g}\right)^2}$$

The flux linkage resulting from the simplified magnetic equivalent is given by:

$$\Phi = N_{ph}\frac{F_j}{R_{gj}+R_{gej}} \tag{18}$$

where F_j is the magnetomotive force of the j-phase, $F_j=N_{ph}I$, R_{gj}, he permeance of the airgap under the pole j, R_{gej} – the equivalent permeance for the rest of the magnetic circuit. The expressions for R_{gj} and R_{gej} are:

$$\begin{aligned} R_{gi} &= \frac{1}{P_0 + P_1\cos(Q_R\theta)} \\ R_{gei} &= \frac{1}{Q_S P_0 - [P_0 + P_1\cos(Q_R\theta)]} \end{aligned} \tag{19}$$

According to Eq. (14), the phase inductance, neglecting the saturation, is presented in Figure 6, against the one obtained with the FE model. As it can be noted, neglecting the saturation, and considering the approximation of the permeance by Eq. (14), the inductance obtained with the MEC is higher than the one obtained with the FE. The effect of the saturation could be taken into account by introducing a saturation function [8].

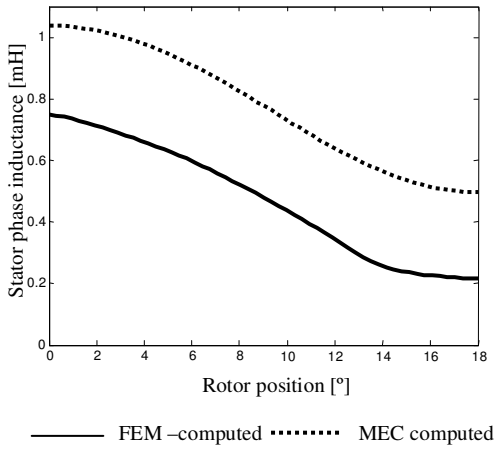

Figure 6. Phase inductance vs rotor position.

The one-phase developed electromagnetic torque results as:

$$\begin{aligned} T = N_{ph}^2 i^2 \frac{Q_R P_1}{2Q_S P_0}\big[&-(Q_S-2)P_0\sin(Q_R\theta) \\ &+ P_1 Q_R \sin(2Q_R\theta)\big] \end{aligned} \tag{20}$$

and is presented in Figure 7. Although the electromagnetic torque equation is also a highly nonlinear function with respect to the rotor position and phase current, a rather accurate prediction (in terms of periodicity, average and maximum values) of torque has been achieved, using (20).

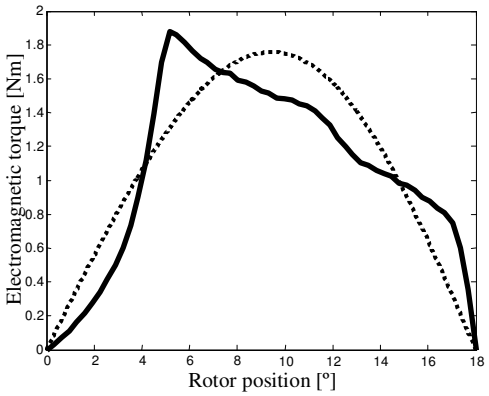

Figure 7. Electromagnetic torque vs rotor position.

C. *Analytical approach*

A mathematical representation of the flux linkage can be developed following the analytical development presented in [7]. According to this approach, the flux linkage can be represented as a Fourier series, as:

$$\Phi(i,\theta) = \Phi_0 + \Phi_1\cos(Q_R\theta) + \Phi_2\cos(2Q_R\theta) \tag{21}$$

with Φ_0, Φ_1, Φ_2 derived as functions of the aligned-position flux linkage Φ_{al}, the unaligned-position flux linkage Φ_{un} and the flux linkage at the midway from aligned to unaligned position Φ_m [7, 8]:

$$\begin{aligned} \Phi_0 &= \frac{1}{2}\left[\frac{1}{2}(\Phi_{al}+\Phi_{un})+\Phi_m\right] \\ \Phi_1 &= \frac{1}{2}(\Phi_{al}-\Phi_{un}) \\ \Phi_2 &= \frac{1}{2}\left[\frac{1}{2}(\Phi_{al}+\Phi_{un})-\Phi_m\right] \end{aligned} \tag{22}$$

The aligned, unaligned and midway position flux linkage can be obtained with the FEM, or could be computed as functions of the stator current. The aligned and midway position phase flux linkage variation function of phase current can be approximated by:

$$\Phi(i) = \frac{i}{ai^2+bi+c} \tag{23}$$

The unaligned-position flux linkage, as shown in Figure 3, can be approximated by a straight line:

$$\Phi(i) = ki \tag{24}$$

where coefficients a, b, c and k are computed via curve fitting procedure based on 2D-FE analysis results.

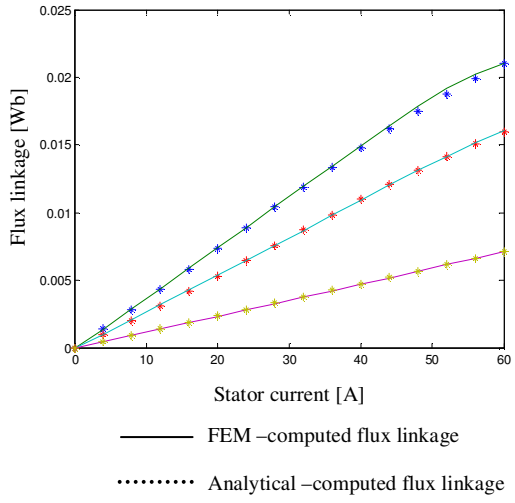

Figure 8. Analytical computed flux linkage vs stator current.

The analytical expression of the electromagnetic torque developed by one phase will result as:

$$T = -\frac{1}{2} Q_R \sin(Q_R\theta)\left[\int_0^i \Phi_{al}\,di - \int_0^i \Phi_{unl}\,di\right] - \\ -\frac{1}{2} Q_R \sin(2Q_R\theta)\left[\int_0^i \Phi_{al}\,di + \int_0^i \Phi_{unl}\,di\right] + \\ + Q_R \sin(2Q_R\theta)\int_0^i \Phi_m\,di \qquad (25)$$

The flux linkage and the electromagnetic torque developed by a stator phase are presented in Figures 8 and 9, against the ones obtained with the FE model.

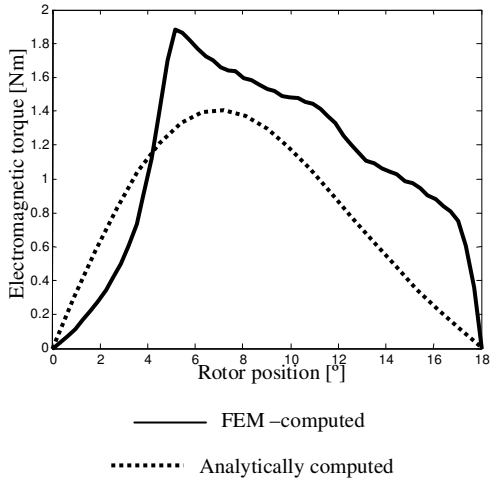

Figure 9. Electromagnetic torque vs rotor position.

It can be observed that the phase flux linkage characteristics obtained by this method closely match those obtained by FEM. Concerning the computation of the torque, the analytical representation is not so accurate in terms of average and maximum values, as the MEC method.

IV. Conclusions

The development of a SRM for an EPAS system has to follow the specification data, the demanded torque-speed curve and some specific constraints: given overall dimension, low voltage feeding supply, wide range of ambient temperature, low motor torque ripple, and fault tolerance. The proposed machine is a 6-phase, 12/10 topology one, suited for fault-tolerant column-type EPAS systems.

After a preliminary design giving the main dimensions of the machine, the computation of parameters has been tackled. According to the mathematical model of the machine, the phase flux linkage expression was derived, either from magnetic equivalent circuit analysis or using an analytical development, taking into account the non-linearity of the magnetic circuit.

The variation of the flux linkage with rotor position was approximated by a Fourier series considering only the first three terms. The coefficients of the terms in the Fourier series were determined via aligned, midway and unaligned FEM computed phase flux linkage.

Magnetic equivalent circuit analysis provided the magnetic equivalent permeance and, the phase inductance. The electromagnetic torque expression was derived through both magnetic circuit analysis and analytical formula. A comparison with the electromagnetic torque computed by FEM validated the obtained expressions.

References

[1] A. Freialdenhoven, "Market view on electric power steering (EPS) systems", Advanced Steering Systems Workshop, Germany, Mai 2006.

[2] D. Iles-Klumpner, "Automotive Permanent Brushless Actuation Technologies", PhD Thesis, Timisoara, Romania, 2005.

[3] R. Krishnan, R. Arumugan, J.F. Lindsay, "Design Procedure for Switched-Reluctance Motors", Industry Applications, IEEE Transactions on 24 No. 3, 1988.

[4] S. Huang, J. Luo, F. Leonardi, T.A. Lipo, "A General Approach to Sizing and Power Density Equations for Comparison of Electrical Machines", IEEE Transactions on Industry Applications, Vol.34, No.1, 1998.

[5] G. Henneberger, I.A. Viorel, "Variable Reluctance Electrical Machines", Shaker Verlag, Aachen, 2001

[6] P. Vijayraghavan, "Design of Switched Reluctance Motors and Development of a Universal Controller for Switched Reluctance and Permanent Magnet Brushless DC Motor Drives", PhD Thesis, Virginia Polytechnic Institute and State University, USA, 2001.

[7] H.P. Chi, R.L. Lin, J.F. Chen, "Simplified flux-linkage model for switched reluctance motors", Electric Power Applications, IEE Proceedings Volume 152, Issue 3, 6 May 2005 Page(s): 577 – 583.

[8] I.A. Viorel, L. Strete, I.F. Soran, "Analytical flux-linkage model of switched reluctance motor", Rev. Roum. Sci. Techn.- Electrotechn. Et Energ, 54, Bucarest, 2009.

[9] ***, "JMAG-Studio 8.3 User Manual, The Japan Research Institut, Ltd. 2005.